MODELLING OF BALLASTED TRACKS: DISCRETE-CONTINUUM APPROACH

Trung Ngoc Ngo[1], Buddhima Indraratna[1]

[1]ARC Training Centre for Advanced Technologies in Rail Track Infrastructure (ITTC-Rail), Centre for Geomechanics and Railway Engineering (CGRE) University of Wollongong Australia
Northfields Ave, Wollongong NSW 2522
Email: trung@uow.edu.au; https://www.uow.edu.au

Keywords: Granular Materials, DEM, Rail Transport, Discrete-Continuum Modelling, Particle Breakage

Abstract: The increasing demand for fast heavy haul services with greater axle loads, as well as high speed commuter trains pose a critical challenge for the stability of tracks built on the problematic ground. The mechanism of ballast degradation and deformation, the understanding of the interaction between discrete ballast aggregates and subgrade media require further insight to improve the existing design guidelines for future high speed commuter and heavier freight trains. This paper presents a study on the load-deformation responses the ballasted rail track subjected to cyclic loading using a novel large-scale track process simulation testing apparatus (TPSTA) and a coupled discrete-continuum modelling approache (coupled DEM-FDM). Experimental studies are carried out to investigate the deformation and degradation responses of ballast subject to cyclic train loading under a given frequency of f=15 Hz. A rigorous coupled model between the discrete element method (DEM) and the finite difference method (FDM) is introduced considering the ballast breakage and influences of the subgrade stiffness. In the coupled discrete-continuum model, the ballast layer is simulated by the discrete element method and the subgrade domain is modelled by the continuum method. Interface elements are introduced to transmit the interacting forces and displacements between the adjoining material media, in which the DEM transfers contact forces to the FDM, and then the FDM transfers displacements (i.e. velocities) back to the DEM. The coupled model is validated by comparing the predicted deformations of ballast with those measured in the laboratory. Contact force distributions, stress contours and corresponding broken bonds (i.e. particle breakage) are captured. These findings are imperative for a more insightful understanding of the micro-mechanical behavior of ballast from the perspective of microstructure characteristics of discrete particle assembliese.

1 INTRODUCTION

In many parts of the world, especially considering the agriculture and mining sectors, the lack of capacity of current transportation infrastructure to support increased freight volume and its efficient mobility (i.e. connecting ports with the regional and rural areas) is of grave concern [1-3]. Railway transportation is designed to supply an efficient, safe and economical mean of transport for commuters and goods [4-7]. This requires ballasted tracks to be designed to cope with varying axle loads, varied train speeds operating on different track and loading conditions [8-10].

A typical ballasted track is usually separated into two groups: superstructure and substructure. The superstructure typically includes rails, sleepers and fastening clips. The substructure includes ballast, subballast (capping), structural fills and subgrade. The superstructure and substructure interact with each other at the interfaces of the sleeper-ballast [11]. The main functions of ballast are to: (i) transmit high stresses at the sleeper-ballast interfaces to the underneath sub-layers at acceptably reduced stress levels; (ii) prevent sleeper movements caused by train loading; (iii) provide adequate drainage capacity for tracks (i.e. increased hydraulic conductivity); and (iv) provide electrical resistance and energy absorption, vibration attenuation and noise absorption for tracks [12]. During train operations, ballast deteriorates due to the particle breakages, the intrusion of fines, and mud-pumping. Consequently, ballast becomes fouled and its shear strength and ability to drain off the water are seriously compromised [13-15]. The use of artificial inclusions including geogrids, geocomposites to reduce the deformation and degradation of ballast has increasingly become attractive in recent decades. Past studies have indicated that the mechanical interlock among a geogrid and surrounding ballast aggregates can prevent the lateral movement and breakage of ballast [16]. However, when the ballast becomes fouled, the interaction mechanism between the aggregates and geogrids will reduce and reinforcement benefit of geogrid can decrease considerably.

The numerical modelling approach has been successfully used to model granular materials which have conventionally been treated as a continuum media. However, owing to the discrete nature of ballast aggregates, the continuum approach (e.g. finite different method) is almost infeasible to accurately capture their micro-mechanical characteristics including fabric anisotropy, angularity and particle breakage. The discrete element method (DEM) firstly introduced by Cundall and Strack [17] has been widely used to study the micro-mechanical behaviour of granular materials [18-20]. The DEM enables to model the discrete nature of ballast grains by providing an insight to micro-scale parameters including particle angularity and shape, interparticle interactions, contact force distributions, particle breakage and fabric changes that are infeasible to determine otherwise. Nevertheless, the high computational cost associated with simulating an assembly of involving a very high number of particles may limit the application of DEM to practical problems. For example, Ngo et al. [21] simulated a typical laboratory test on fouled ballast and it required almost 500 hours (running on a high performance workstation) to complete simulations for large-scale direct shear tests. Given the exceedingly great computational cost required to solve a practical rail track embankment in DEM, this study develops a combined discrete-continuum approach to fully appreciate the advantages of both the discrete and continuum methods and meanwhile to mitigate their respective drawbacks.

2 LARGE-SCALE LABORATORY TEST

2.1 Rail process simulation testing apparatus (RPSTA)

To examine the load-deformation responses of railway ballast subjected to cyclic train loading, laboratory tests using the innovative rail process simulation test apparatus (RPSTA) were conducted to simulate realistic Australian railway tracks [22-23]. The RPSTA can accommodate a ballast assembly of 800 mm long, 600 mm wide and 600 mm high (Fig. 1). A system of hinge and ball bearings was used to allow ballast aggregate to displace during the tests at minimum frictional resistance. Settlement pegs were placed at each of the ballast/sleeper and capping/ballast interfaces to record vertical settlements. Cyclic train loading was simulated by a servo hydraulic actuator and applied on ballast layer by a concrete

sleeper connected with a steel ram. During the testing, lateral movements of the four vertical walls were automatically recorded by electronic potentiometers. Vertical stresses generated at the interfaces of sleeper-ballast and ballast-capping were measured by pressure cells. All instrumentations were calibrated and connected to an electronic data logger (AMD-DT800) to accurately record all vertical, lateral displacements and stress distributions at desired time intervals during the the testing progress.

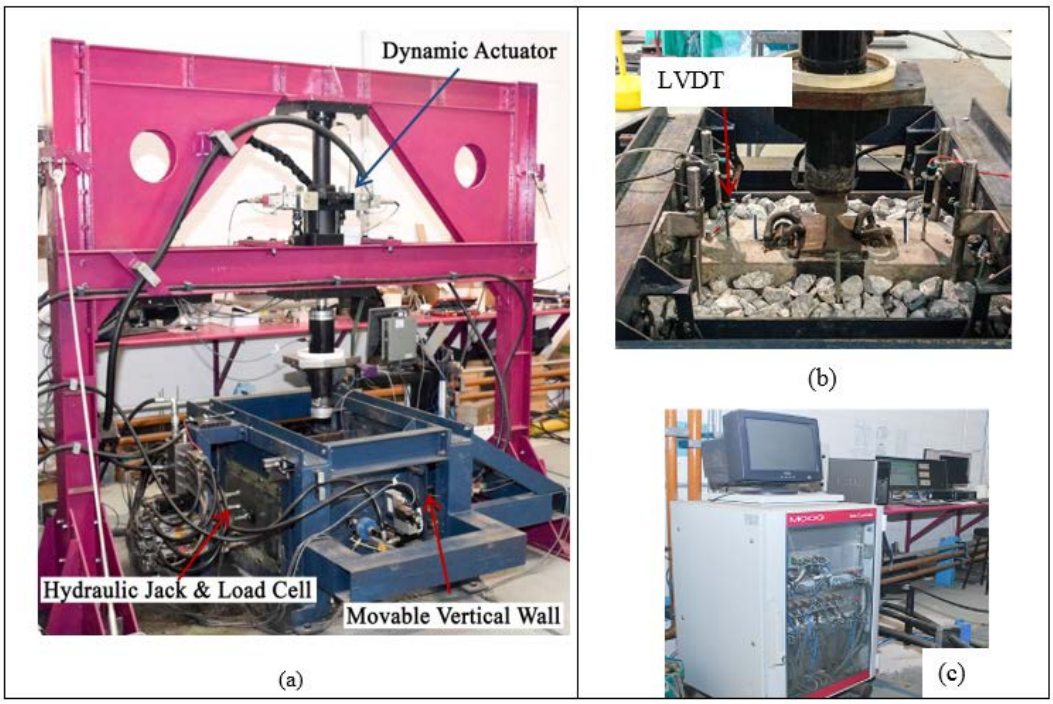

Figure 1: a) Rail process simulation testing apparatus; (b) Ballast tesing sample; (c) Data acquisition system

2.2 Materials tested and testing procedure

Fresh ballast aggregates were taken from Bombo quarry, near Wollongong, Australia. The ballast was then cleaned and sieved according to the Australia Standards, AS 2758.7 [24]. To represent field conditions, compacted coarse sand, having a thickness of 50 mm, compacted at 8 % moisture contents to a given unit weight of 18.5 kN/m^3, was positioned at the bottom of the test chamber to simulate a subgrade layer. A 100mm thick layer of capping consisting of the sand-gravel mixture was compacted to a given unit weight of 19.8 kN/m^3, placed on top of the subgrade layer, followed by 300 mm thick ballast layer compacted to a unit weight of 15.5 kN/m^3.

After preparing the assembly, a lateral pressure of σ_2=15 kPa, corresponding to lateral confinement provided by shoulder ballast in the field was imposed. An initial vertical load of 5 kN was then placed upon to stabilise the sleeper and ballast, and to work as a reference point (datum) for all lateral and settlement measurements. The cyclic load was applied through a servo hydraulic actuator with a maximum load of 70 kN, at a given frequency of f=15 Hz. These load magnitude and frequency provide similar average contact stress at sleeper/ballast of 25 tonnes/axle train loading travelling at an approximate speed of 80 km/h, which are typical parameters for Australian trains. A total of N=500,000 load cycles was carried out in each test, but the tests were paused at specific cycles, N to record readings from settlement pegs. Experimental results showed that ballast aggregates exhibited a significant deformation in

initial loading cycles, continued by slightly increased deformation and then kept almost stable to the end of the test. Some of the measured test data is used herein to calibrate and validate a coupled DEM-FDM model.

3 COUPLED DEM-FDM MODELLING OF BALLASTED TRACKS

A coupled DEM-FDM model introduces in this study to take advantages of each modelling scheme and to provide a viable approach to model ballasted track embankment. The DEM was used to simulate ballast aggregates where the shape and size of realistic ballast grains were simulated using clusters of bonded circular particles (Fig. 2a). It is noted that the breaking of these bonds within a cluster was considered to represent ballast breakage. Micro-mechanical parameters adopted for ballast grains and walls used in DEM were obtained by calibrating with laboratory test data. A continuum-based method (finite difference method-FDM) was used to model the subgrade and capping layer, having a thickness of 150 mm to mimic a capping formation in the field (Fig. 2b). Principally, coupling between the DEM and FDM can be facilitated at the ballast-capping interface by: (i) treating nodal displacements of the finite elements as boundary conditions (i.e. applied wall velocities) for discrete particles; and (ii) by applying the forces acting on the discrete elements as force boundary conditions to the finite element grids. The couple DEM-FDM model was calibrated by laboratory test data measured from the rail process simulation testing apparatus. The coupled DEM-FDM model was then be used to perform cyclic tests subjected to varying loading frequencies, f=10-40 Hz and run up to N=10,000 cycles.

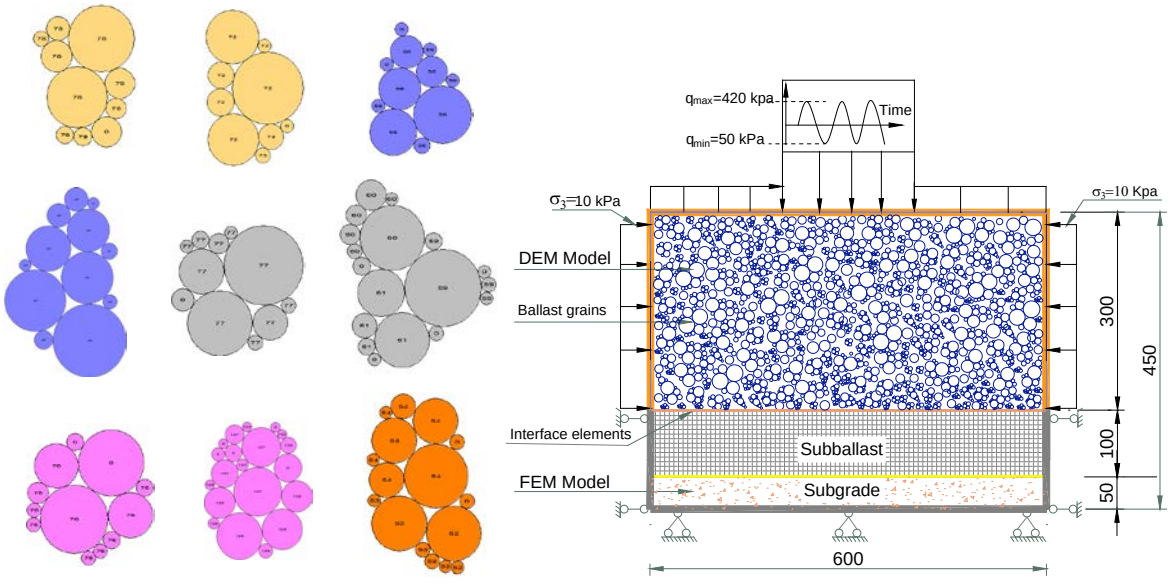

(a) (b)

Figure 2: a) Simulated ballast shapes in DEM; (b) Geometry of the coupled DEM-FDM model

The interaction between ballast grains (DEM domain) and capping/subgrade layers (FDM domain) were facilitated by transferring of forces and displacements [25]. The schematic diagram of exchanging of contact forces (F_n, F_s) and velocity ($\dot{X}_i^{[E]}$) between the discrete

particles and continuum elements at their interfaces is presented in Figure 3a. The superscripts *C*, *E*, and *P* represent contacts, elements, and particles, respectively.

Contact forces at interfaces are calculated as:

$$F_i^{[C]} = F_n^{[C]} + F_S^{[C]} \tag{1}$$

where, normal force ($F_n^{[C]}$) and increment of shear force ($\Delta F_s^{[C]}$) are computed as:

$$F_n^{[C]} = K^n U^n n_i \;; \quad \text{and} \quad \Delta F_s^{[C]} = -K^s\left(\Delta X_i^{[C]} - \Delta X_i^{[C]} n_i\right) \tag{2}$$

Resultant forces and moments acting on particles at the interface can be estimated as:

$$F_i^{[P]} \leftarrow F_i^{[P]} - F_i^{[C]}; \text{ and } M_i^{[P]} \leftarrow M_i^{[P]} - e_{ijk}\left(X_j^{[C]} - X_j^{[P]}\right)F_k^{[C]} \tag{3}$$

Relative contact velocity (displacement) at the interface (V_i) can be obtained by:

$$V_i = \dot{X}_{i,E}^{[C]} - \dot{X}_{i,E}^{[P]} = \dot{X}_{i,E}^{C} - \left[\dot{X}_i^{[P]} + e_{ijk}\omega_j^{[P]}(X_k^{[C]} - X_k^{[P]})\right] \tag{4}$$

where, $\dot{X}_{i,E}^{[P]}$ and $\dot{X}_{i,E}^{[C]}$ are the velocities of particles and elements, respectively. $\dot{X}_i^{[P]}$ and $\omega_j^{[P]}$ are translation and rotation of a particle, and e_{ijk} is a permutation symbol.

Velocity (displacement) of continuum elements at interfaces can be calculated as:

$$\dot{X}_{i,E}^{[C]} = \sum N_j \dot{X}_{i,E}^{j} \tag{5}$$

where, N_j is the shape function, given by: $N_j = (1+\xi_o)(1+\eta_o)/4$, $j = 1,2,3,4$; and $\xi_o = \xi_i \xi$, $\eta_o = \eta_i \eta$; ξ_i and η_i are local coordinates of nodes. At the interface, the shear and the normal contact forces are distributed to the nodal force, $F_i^{[E,j]}$ following to the shape function N_j, given by:

$$F_i^{[E,j]} = F_i^{[E]} + F_i^{[C]} N_j \tag{6}$$

The time step, Δt was selected to ensure numerical stability conditions, given by: $\Delta t_{ct} \le \min\left\{\Delta t_{dcr}, \Delta t_{fcr}\right\}$, in which, $\Delta t_{dcr} = \sqrt{m^d / K^n}$ is the critical time step of DEM region; m^d and K^n are the mass and stiffness of ballast particle; $\Delta t_{fcr} = L_{\min} / C_f$ is the critical time step of FDM region; $L_{\min}$ = minimum length of finite elements; $C_f = \sqrt{E_f(1-\mu_f)/[\rho_f(1-\mu_f)(1-2\mu_f)]}$ is the velocity of elastic wave; E_f, μ_f, and ρ_f are Young's modulus, Poisson's ratio, and unit weight of capping, respectively.

3.1 Distributing contact forces and moment at interfaces

It is noted that an interface element only receives forces at their nodes (i.e. F_{XA}, F_{YA}, F_{XB}, F_{YB}). Thereby, it is essential to transfer forces and moments (M) from a discrete particle (F_X, F_Y and M) to a continuum element, as described in Figure 3b. Considering the force equilibrium on horizontal and vertical directions, it can be derived as:

$$F_X = F_{X_A} + F_{X_B} \qquad \text{and} \qquad F_Y = F_{Y_A} + F_{Y_B} \tag{7}$$

Considering moment equilibrium at the centre (C) of an interface element, results in:

$$M = F_{Y_A} \times (X_A - X_C) + F_{Y_B} \times (B - X_C) - F_{X_A} \times (Y_A - Y_C) - F_{X_B} \times (Y_B - Y_C) \quad (8)$$

Equations (7) can be expressed as:

$$F_X = F_{X_A} + F_{X_B} = \Omega \times F_X + (1 - \Omega) \times F_X \quad (9)$$

$$F_Y = F_{Y_A} + F_{Y_B} = \Omega \times F_Y + (1 - \Omega) \times F_Y$$

Substituting Equation (9) to Equation (8), results in:

$$M = \Omega \times F_Y \times (X_A - X_C) + (1 - \Omega) \times F_Y \times (X_B - X_C) - \Omega \times F_X \times (Y_A - Y_C) - (1 - \Omega) \times F_X \times (Y_B - Y_C) \quad (10)$$

Rearranging Equation (10), results in:

$$\Omega = \frac{M - F_Y \times (X_B - X_C) + F_X \times (Y_B - Y_C)}{F_Y \times (X_A - X_B) - F_X \times (Y_A - Y_B)} \quad (11)$$

Equation (11) can be used together with Equations (7-8) to distribute forces and moment from the DEM zone to the FDM zone at elements' nodes to implement the coupling process.

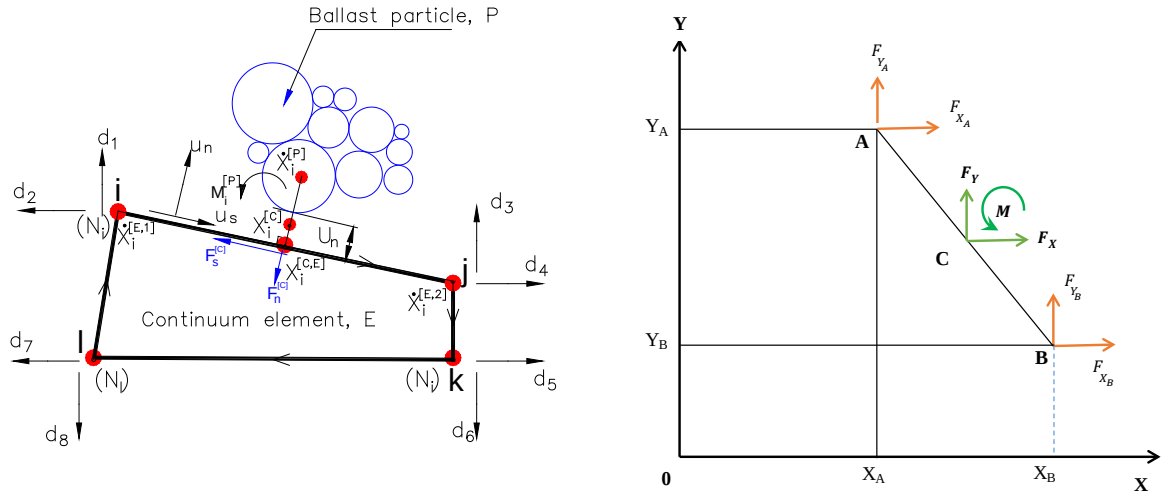

Figure 3: a) Interaction of a discrete particle and a continuum element; and (b) Diagram of transferring forces and moment from DEM to FDM.

4 RESULTS AND DISCUSSION

4.1 Cyclic stress-strain responses

Figure 4 shows the predicted cyclic stresses with accumulated axial strains obtained from the coupled DEM-FDM model at varying load cycles. It is seen that the predicted axial strains increase remarkably up to around 3% within the first 1000 load cycles, followed by slightly increased axial strains up to N=5,000 cycles, and then remained relatively stable to the end (N=10,000 cycles). Indeed, the cyclic hysteresis loops become remarkably smaller with an

increased number of cycles, implying that the ballast specimen through cyclic densification starts responding more elastically with increased time. The area of the hysteresis loop is also identical to the one measured in laboratory tests reported elsewhere [26-28].

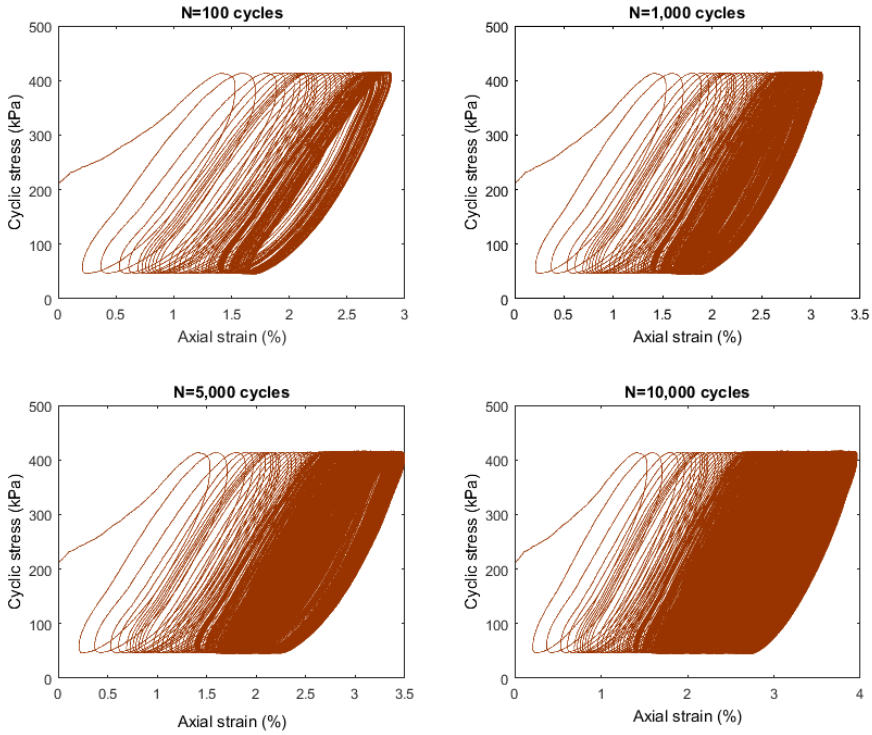

Figure 4: Simulated applied cyclic stress versus axial strain at increased load cycle, *N*

4.2 Ballast breakage responses

It is noted in this study that the disconnection of bonds among a cluster of particle are approximately represented the breakage of ballast in the current coupled DEM-FDM analysis. Figure 5 shows the images of the evolution of bond breakage (numbers and places of breakages) at varying number of cyclic loads (from N=100-10,000 cycles) under a specific loading frequency, f=15 Hz. Within the first 100 cycles, the large amount of broken bonds occurs right underneath the loading plate due to induced large contact forces (Fig. 5a). With an increase in cyclic loading cycles, there is an increased number of broken bonds (Figs. 5b-f) and there was rearrangement of particles (i.e. particles get compacted and ceased from further breaking), which resulted in more uniform contact force distributions in the vertical direction (i.e. major principal directions of stresses). It is observed that the evolutions of broken bonds have an identical trend to the increased amount of ballast breakage that was measured from the laboratory testing data by Indraratna et al. [23]. This observation explains that the evolution of contact forces in the ballast assembly is a dynamic process, remarkably governed by the ballast breakage [29-30]. Figure 5g shows typical locations and the movements of broken grains under cyclic loads where the bonds are separated and the

corresponding aggregates are moving away from each other, representing particle breakage.

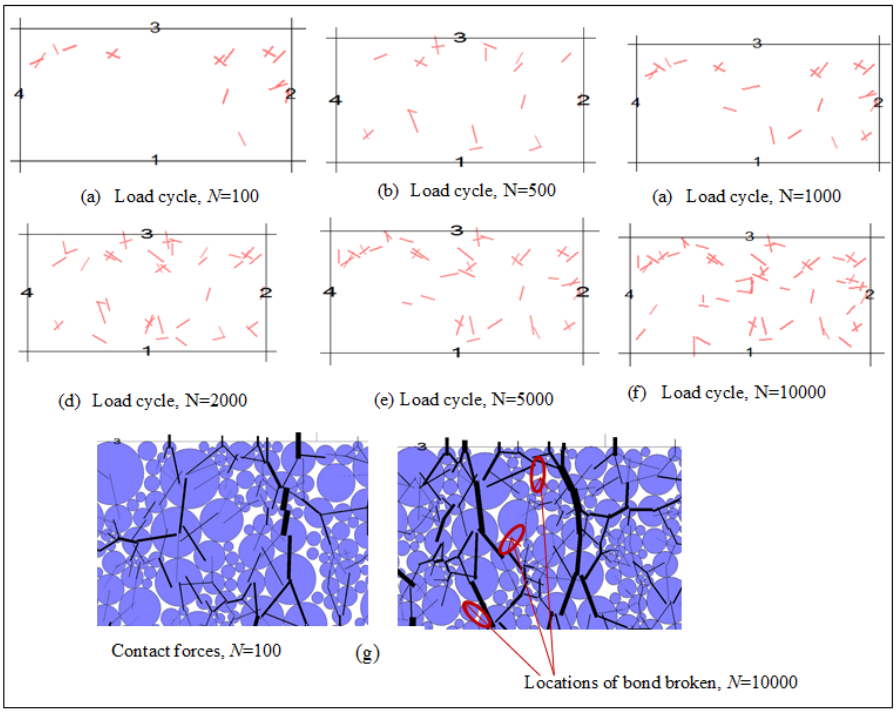

Figure 5: Predicted number of bond breaking at varied load cycles: *N*=100; (b) *N*=500; (c) *N*=1000; (d) *N*=2000; (e) *N*=5000; (f) *N*=10000; (g) locations of bond broken

4.3 Contact forces and stress analysis

The applied cyclic load transmits to the discrete ballast particles in a form of contact force chains where the pattern fabric of forces vary with packing structure and substantial controls the deformation and strength behaviour of the ballast assembly [20, 21]. Figure 6 presents the inter-particle contact forces of a simulated ballast assembly together with vertical stress contours of underlying layers captured at different load cycles of *N*=10, *N*=1000 and *N*=5000 load cycles. It is observed that the majority of contact forces are distributing in a vertical direction which is transmitting the applied cyclic loads downwards the underlying layers. In addition, the force distributions in the DEM region shows heterogeneous, where the number of contacts and maximum forces substantially change with load cycles. These forces create the deformation of the assembly (i.e. vertical and lateral displacements) and the breakage of contact bonds (i.e. particle breakage). Upon repeated cyclic loading, there are high concentrations of contact forces occurring right underneath the loading plate (wall No. 3), and around wall edges, while a significant part of the applied load is transmitted vertically to the underneath subgrade (Figs. 6b-c). Compressive stress in the subgrade is higher primarily at the interface areas that are directly in contact with the ballast aggregates, whereby it is predicted to considerably decrease with depth.

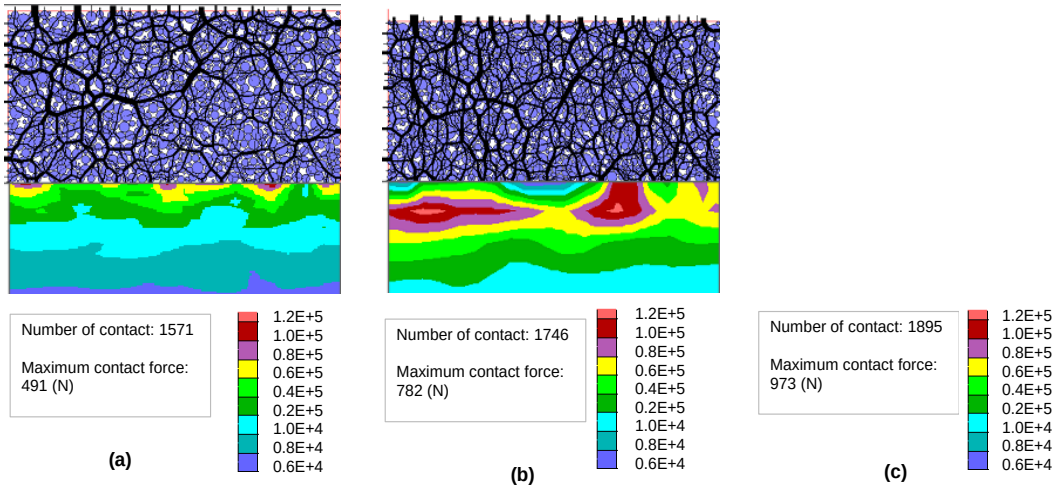

Figure 6. Distribution of contact forces and vertical stress contour developed in discrete and continuum media at varying load cycles; (a) *N*=10 cycles; (b) *N*=1000 cycles; and (c) *N*=5000

5 CONCLUSIONS

Large-scale rail process simulation testing apparatus (RPSTA) tests were performed to examine the load-deformation responses of ballast subjected to cyclic train loadings. Experimental results implied that the ballast showed a significant deformation in initial loading cycles, continued by slightly increased deformation and then kept almost stable to the end of the test. A coupled discrete-continuum approach was introduced to examine the load-deformation behaviour of ballast where the discrete grains were simulated by the DEM and the continuum subgrade/capping media was simulated by FDM. Irregularly shaped ballast aggregates were simulated in the DEM by bonding of pre-determined amount of balls together to mimic appropriate particles' angularity, size and shape. The coupling between discrete and continuum domains was implemented using a developed mathematical approach to transfer forces and displacements at interface elements.

Measured data on the load-deformation responses of ballast was used to calibrate and validate the coupled DEM-FDM model subjected to cyclic loading. Evolutions of contact forces and contours of stresses developed in the ballast assemblies at varied stages of cyclic loading were captured. Results showed that the contact force distributed non-uniformly across the specimens where the maximum forces happening right beneath sleepers, leading to an increased number of broken bonds. This study provided further insight into breakage-induced deformation of ballast as influenced by microstructural characteristics of discrete particle assemblies.

6 ACKNOLEDGEMENTS

This research was conducted by the Australian Research Council Industrial Transformation Training Centre for Advanced Technologies in Rail Track Infrastructure (IC170100006) and funded by the Australian Government. The authors are grateful to A/Prof Cholachat Rujikiatkamjorn for various assistance and helpful discussion. Assistance during the laboratory work provided by Cameron Neilson and Duncan Best are also gratefull apreciated.

REFERENCES

[1] Boler, H., Mishra, D., Hou, W. and Tutumluer, E. (2018). Understanding track substructure behavior: Field instrumentation data analysis and development of numerical models. *Transportation Geotechnics*, 17, 109-121.

[2] Esveld, C. (2001). Modern railway track, MRT Press, The Netherlands.

[3] Powrie, W., Yang, L.A. and Clayton, C.R.I. (2007). Stress changes in the ground below ballasted railway track during train passage. *Proceedings of the Institution of Mechanical Engineers: Part F: Journal of Rail and Rapid Transit*, 247-261.

[4] Selig, E.T. and Waters, J.M. (1994). Track geotechnology and substructure management, Thomas Telford, London.

[5] Wang, H.-L., Cui, Y.-J., Lamas-Lopez, F., Dupla, J.-C., Canou, J., Calon, N., Saussine, G., Aimedieu, P. and Chen, R.-P. (2018). Permanent Deformation of Track-Bed Materials at Various Inclusion Contents under Large Number of Loading Cycles. Journal of Geotechnical and Geoenvironmental Engineering, 144(8), 04018044.

[6] Leng, W., Xiao, Y., Nie, R., Zhou, W. and Liu, W. (2017). Investigating Strength and Deformation Characteristics of Heavy-Haul Railway Embankment Materials Using Large-Scale Undrained Cyclic Triaxial Tests. *International Journal of Geomechanics*, 17(9), 04017074.

[7] Ishikawa, T., Sekine, E. and Miura, S. (2011). Cyclic deformation of granular material subjected to moving-wheel loads. *Canadian Geotechnical Journal*, 48(5), 691-703.

[8] Biabani, M.M., Ngo, N.T. and Indraratna, B. (2016). Performance evaluation of railway subballast stabilised with geocell based on pull-out testing. *Geotextiles and Geomembranes*, 44(4), 579-591.

[9] Sun, Q., Indraratna, B. and Ngo, N.T. (2018). Effect of increase in load and frequency on the resilience of railway ballast., 0(0), 1-8.

[10] McDowell, G.R., Lim, W.L., Collop, A.C., Armitage, R. and Thom, N.H. Laboratory simulation of train loading and tamping on ballast. *Proceedings of the Institution of Civil Engineers: Transport*, 158(TR2), 89-95.

[11] Ngo, N.T., Indraratna, B., Ferreira, F.B. and Rujikiatkamjorn, C. (2018). Improved performance of geosynthetics enhanced ballast: laboratory and numerical studies. *Proceedings of the Institution of Civil Engineers-Ground Improvement*, 171(4), 202-222.

[12] Priest, J.A., Powrie, W., Yang, L., Grabe, P.J. and Clayton, C.R.I. (2010). Measurements of transient ground movements below a ballasted railway line. *Géotechnique*, 60(9), 667–677.

[13] Indraratna, B., Ngo, N.T. and Rujikiatkamjorn, C. (2011). Behavior of geogrid-reinforced ballast under various levels of fouling. *Geotextiles and Geomembranes*, 29(3), 313-322.

[14] Tutumluer, E., Dombrow, W. and Huang, H. (2008). Laboratory characterization of coal dust fouled ballast behaviour. AREMA 2008 Annual Conference & Exposition, Salt Lake City, UT, USA.

[15] Danesh, A., Palassi, and Mirghasemi. (2018). Effect of sand and clay fouling on the shear strength of railway ballast for different ballast gradations. *Granular Matter*, 20(3), 51.

[16] Ngo, N.T., Indraratna, B. and Rujikiatkamjorn, C. (2017). A study of the geogrid–subballast interface via experimental evaluation and discrete element modelling. *Granular Matter*, 19(3), 54: 51-16.

[17] Cundall, P.A., Strack O.D.L. (1979). A discrete numerical model for granular assemblies. *Géotechnique* 29(1), 47-65.

[18] Tutumluer, E., Huang, H. and Bian, X. (2012). Geogrid-aggregate interlock mechanism investigated through aggregate imaging-based discrete element modeling approach. *International Journal of Geomechanics*, 12(4), 391-398..

[19] Ngo, N.T., Indraratna, B. and Rujikiatkamjorn, C. (2017). Simulation Ballasted Track Behavior: Numerical Treatment and Field Application. *ASCE-International Journal of Geomechanics*, 17(6), 04016130..

[20] O'Sullivan, C. (2011). Particulate Discrete Element Modelling: A Geomechanics Perspective, Spon press, London.

[21] Ngo, N.T., Indraratna, B. and Rujikiatkamjorn, C. (2014). DEM simulation of the behaviour of geogrid stabilised ballast fouled with coal. *Computers and Geotechnics*, 55, 224-231.

[22] Navaratnarajah, S.K., Indraratna, B. and Ngo, N.T. (2018). Influence of under sleeper pads on ballast behavior under cyclic loading: experimental and numerical studies. *Journal of Geotechnical and Geoenvironmental Engineering*, 144(9), 04018068.

[23] Indraratna, B., Ngo, N.T. and Rujikiatkamjorn, C. (2013). Deformation of coal fouled ballast stabilized with geogrid under cyclic load. *Journal of Geotechnical and Geoenvironmental Engineering*, 139(8), 1275-1289.

[24] AS:2758.7: (2015). Aggregates and rock for engineering purposes, Part 7. Railway Ballast. Standard Australia, Australia.

[25] Itasca (2016). Particle flow code in three dimensions (PFC3D). Itasca Consulting Group, Inc., Minnesota.

[26] Lamas-Lopez, F., Cui, Y.-J., Calon, N., Costa D'Aguiar, S., Peixoto De Oliveira, M. and Zhang, T. (2016). Track-bed mechanical behaviour under the impact of train at different speeds. *Soils and Foundations*, 56(4), 627-639.

[27] Wang, H.L., Cui, Y.J., Lamas-Lopez, F., Dupla, J.C., Canou, J., Calon, N., Saussine, G., Aimedieu, P. and Chen, R.P., 2017. Effects of inclusion contents on resilient modulus and damping ratio of unsaturated track-bed materials. *Canadian Geotechnical Journal*, 54(12), pp.1672-1681.

[28] García-Rojo, R., Alonso-Marroquín, F. and Herrmann, H.J., 2005. Characterization of the material response in granular ratcheting. *Physical Review E*, 72(4), p.041302.

[29] Einav, I. (2007). Breakage mechanics—Part II: Modelling granular materials. *Journal of the Mechanics and Physics of Solids*, 55(6), 1298-1320.

[30] Donohue, S., O'Sullivan, C. and Long, M. (2009). Particle breakage during cyclic triaxial loading of a carbonate sand. *Géotechnique*, 59(5), 477-482.